Ramsey effects in coherent resonances at closed transition $F_g = 2 \rightarrow F_e = 3$ of ^{87}Rb

2012 J. Phys. B: At. Mol. Opt. Phys. 45 245502

(http://iopscience.iop.org/0953-4075/45/24/245502)

J. Phys. B: At. Mol. Opt. Phys. **45** (2012) 245502 (8pp) doi:10.1088/0953-4075/45/24/245502

Ramsey effects in coherent resonances at closed transition $F_g = 2 \rightarrow F_e = 3$ of ^{87}Rb

Z D Grujić, M M Lekić, M Radonjić, D Arsenović and B M Jelenković

Institute of Physics, University of Belgrade, Pregrevica 118, 11080 Belgrade, Serbia

E-mail: milan.radonjic@ipb.ac.rs

Received 22 August 2012, in final form 8 October 2012
Published 30 November 2012
Online at stacks.iop.org/JPhysB/45/245502

Abstract

Experimental and theoretical investigations show the strong effect of the pump beam, spatially separated from the probe beam, on the probe's electromagnetically induced absorption (EIA) and nonlinear magneto-optical rotation (NMOR). Linearly polarized pump and probe laser beams are locked to the $F_g = 2 \rightarrow F_e = 3$ transition of the ^{87}Rb D_2 line and pass a vacuum Rb gas cell coaxially. We show that the observed narrowing of EIA and NMOR resonances is due to the Ramsey effect. Linewidths of the resonances decrease when the size of the dark region between pump and probe lasers increases. Variation of the angle between pump and probe linear polarizations strongly influences the phases of atomic coherences generated by the pump beam and consequently the line-shapes of the probe EIA and NMOR resonances. Complete change of the resonance sign is possible if the phases of the ground state coherences, $\Delta m_g = 2$, are altered by π. The central EIA fringe becomes less pronounced if the probe intensity increases, due to the larger probe contribution to atomic evolution. Ramsey-like interference is a manifestation of the evolution of ground state Zeeman coherences, required for EIA, in the dark region in the presence of a small magnetic field.

(Some figures may appear in colour only in the online journal)

1. Introduction

In the work of Akulshin *et al* [1], a new kind of resonance was observed, one in which atomic coherence produces an increase of laser absorption. This coherent phenomena is termed electromagnetically induced absorption or EIA. Conditions for observing EIA have been recently identified: a narrow absorption resonance can be obtained when the laser frequency is scanned across a degenerate two-level transition such that $F_g \rightarrow F_e = F_g+1$, where F_g and F_e are total angular momentum quantum numbers of hyperfine levels of ground and excited states, respectively. It is worth mentioning that Kazantsev *et al* [2] theoretically predicted that optical pumping in the case of such transitions leads to an enhanced absorption of the medium. It is now well known that EIA is a multilevel effect, meaning that the degeneracy of the ground level is necessary. In comparison to electromagnetically induced transparency (EIT) [3] EIA has an opposite sign of resonance. Unlike EIT, which is due to coherent population trapping (CPT) and ground level dark states [4], EIA has not been associated with a particular coherent superposition of atomic ground states. While both EIT and CPT were intensely investigated over the past decade, this is not the case for EIA. A better knowledge of the phenomena is necessary, including a better understanding of excitation and emission processes that lead to the development of EIA.

The first observations of EIA were performed by perpendicularly polarized pump and probe lasers, interacting with a cycling degenerate two-level transition in which $F_e = F_g + 1$ and $F_g > 0$ [1, 5]. In later experiments, EIA was also found in non-cycling degenerate two-level systems [6, 7]. Both two-photon resonances in a bichromatic light field (pump–probe spectroscopy) and magneto-optical resonances in the Hanle configuration have been explored. The influence of various parameters like laser intensity, light ellipticity and magnetic fields on EIA amplitudes and linewidths was studied in [8–11].

Assuming the simplest system presenting EIA, a four-level N-atomic system of a near degenerate two-level atom, Taichenachev *et al* [13] obtained an analytic expression for the probe light absorption. A direct link between the efficiency of spontaneous coherence transfer and the appearance of EIA indicates that the Zeeman coherence, after being developed in the excited level, is transferred to the ground level

by spontaneous emission. Analytic expressions of different perturbation orders for Zeeman and optical coherences and populations have shown such ordering of events in the development of EIA [14].

EIA media have some similarities but also differences from EIT media. Since these two coherent phenomena have different origins, their temporal behaviour is different, as given in [15]. Slower development of EIA and its consequent narrowing after turning on the excitation pulse was notable in comparison with EIT. EIA media have a steep anomalous dispersion that is related to subluminal light propagation, as demonstrated in [16]. As a consequence, in EIA media light pulses can also be stored and retrieved like in EIT media, but only the storage of a smaller part of the initial pulse is possible [17]. In some open atomic systems, minor changes of the pump laser Rabi frequency can transform EIT to EIA (and vice versa) [18]. A modest change of the buffer gas cell's temperature can alter the sign of the transmission resonance from positive (EIT) to negative (EIA) [12].

Ramsey's method of separated fields is often used in atomic and molecular beam experiments [19]. Ramsey fringes that are induced by the two spatially or temporally separated excitation fields lead to a considerable narrowing of the corresponding resonances. In this work, we test if the Ramsey effects of separated pump and probe laser beams can be effective for narrowing EIA as they are for EIT. Repeated interaction of coherently prepared alkali-metal atoms with a pair of laser fields in Raman resonance leads to a strong Ramsey narrowing of EIT in cells with buffer gas [20, 21], and in vacuum gas cells if a specific pump–probe laser beam geometry is used [22, 23]. The Ramsey effects on EIA were recently explored in gas cells with anti-relaxation coating experimentally [24] and, using a four-level N-atomic system, theoretically [25]. We look for the Ramsey effects introduced by separated excitation fields in an EIA medium in a vacuum gas cell without anti-relaxation coating by measuring and calculating the probe's transmission and nonlinear magneto-optical rotation (NMOR) when the laser fields couple the $F_g = 2 \rightarrow F_e = 3$ transition of the ^{87}Rb D_2 line. In V atomic schemes supporting EIA, polarization rotation has the opposite sign to that in EIT atomic systems, e.g. Λ or M systems. There have been numerous studies of NMOR in EIT media in buffer-gas-free vapour cells and without anti-relaxation coating [26–29]. A change of the NMOR sign in the case of the closed transition $F_g = 4 \rightarrow F_e = 5$ of the Cs D_2 line was first reported in [27].

In our work, we use a pump laser beam to coherently prepare the atoms and a spatially separated probe laser beam to check the pump-induced atomic coherence. We studied the Ramsey effects on narrowing EIA and NMOR, theoretically and experimentally, using a similar pump–probe geometry as in [22]. Both pump and probe laser beams are linearly polarized and resonant to the closed transition, $F_g = 2 \rightarrow F_e = 3$ in ^{87}Rb. EIA measurements were carried out by monitoring the probe beam's transmission. NMOR of the linear probe polarization, for a given pump polarization, is obtained using a balanced polarimeter. The measurements were performed as a function of the external axial magnetic field for different angles between the electric vectors of the pump and probe beams. Obtained EIA and NMOR line-shapes are compared with the results of the theoretical model. The model solves time-dependent optical Bloch equations for the density matrix elements for all sublevels of the $F_g = 2 \rightarrow F_e = 3$ transition. The atomic state evolution is calculated when an atom passes the pump, the dark region and the probe beam. The probe's total transmission was calculated after averaging over all atom velocity components parallel and perpendicular to the laser beam and over all possible atomic trajectories. The probe beam's transmission and polarization rotation are obtained from the calculated change of the probe's electric field due to the Rb vapour polarization.

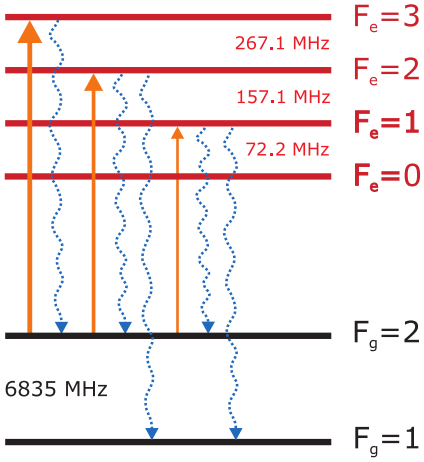

Figure 1. Energy level diagram for D_2 line transitions considered in the theoretical model. Solid arrows pointing up represent the transitions induced by the laser, while dotted wavy arrows pointing down correspond to possible spontaneous emission channels from excited levels. Frequency differences between adjacent hyperfine levels are shown.

2. Theory

We used a density-matrix formalism to model the dynamics of the interaction between Rb atoms and spatially separated pump and probe laser beams. Figure 1 shows a Rb D_2 line atomic level diagram, the hyperfine levels either coupled by the laser light, or populated via spontaneous emission.

The external magnetic field **B**, along the propagation direction of the laser beam, splits the adjacent Zeeman sublevels by the amount $\mu_B g_F B$, where μ_B is the Bohr magneton and g_F is the gyromagnetic factor of the level. The temporal evolution of the atomic density matrix is obtained from time-dependent optical Bloch equations for a moving atom

$$\frac{\mathrm{d}\hat{\rho}}{\mathrm{d}t} = -\frac{\mathrm{i}}{\hbar}[H_{\mathrm{atom}}(B) + H_{\mathrm{int}}(t), \hat{\rho}] + \left(\frac{\mathrm{d}\hat{\rho}}{\mathrm{d}t}\right)_{\mathrm{SE}}, \qquad (1)$$

where

$$H_{\mathrm{atom}}(B) = \sum_j \hbar\omega_j(B)|g_j\rangle\langle g_j| + \sum_k \hbar\omega_k(B)|e_k\rangle\langle e_k|, \qquad (2)$$

is the atomic Hamiltonian corresponding to ground (excited) states $|g_j\rangle$ ($|e_k\rangle$) with Zeeman-shifted energies $\hbar\omega_j(B)$ ($\hbar\omega_k(B)$). The laser–atom interaction is given by

$$H_{\mathrm{int}}(t) = -\sum_{j,k} \mathbf{E}(t) \cdot \mathbf{d}_{jk}(|g_j\rangle\langle e_k| + |e_k\rangle\langle g_j|), \qquad (3)$$

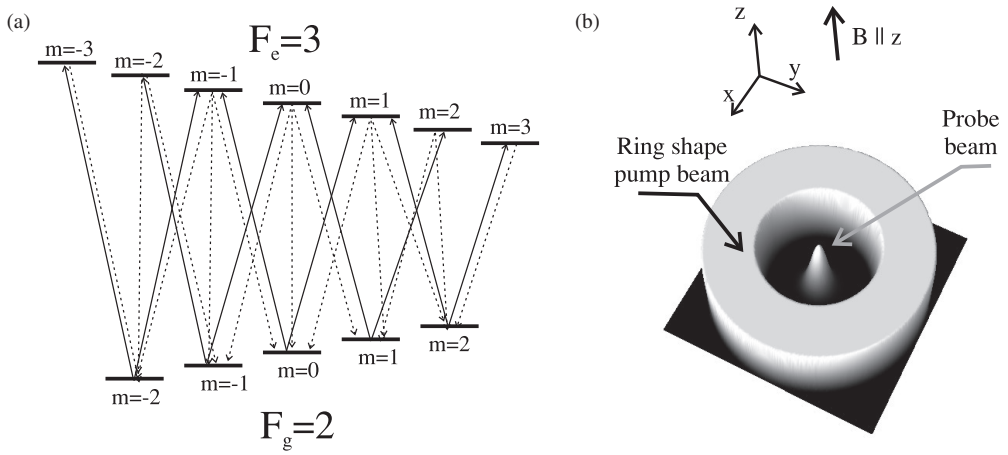

Figure 2. (a) The energy level diagram for magnetic sublevels of the $F_g = 2 \rightarrow F_e = 3$ transition and (b) pump and probe laser beam radial profiles used in the theoretical model. In (a) solid lines represent transitions induced by the linearly polarized laser fields, while dotted lines correspond to possible spontaneous emission channels from excited levels.

where $\mathbf{E}(t)$ is the time-dependent electric field of the laser seen by the atom and $\mathbf{d}_{jk}$ is the atomic electric dipole moment for the transition between states $|g_j\rangle$ and $|e_k\rangle$. Spontaneous emission is treated using the Lindblad-form term

$$\left(\frac{\mathrm{d}\hat{\rho}}{\mathrm{d}t}\right)_{\mathrm{SE}} = \sum_m 2\Gamma_m\hat{\rho}\Gamma_m^\dagger - \Gamma_m^\dagger\Gamma_m\hat{\rho} - \hat{\rho}\Gamma_m^\dagger\Gamma_m, \tag{4}$$

where Γ_m are operators related to dipole transitions from the excited to ground state manifold. Although the laser is frequency locked to the $F_g = 2 \rightarrow F_e = 3$ transition, due to Doppler broadening, the excited hyperfine levels $F_e = 2$ and $F_e = 1$ are also laser-coupled and therefore have to be included in the calculations. Equations for density matrix elements related to the $F_g = 1$ ground level are excluded since that level is not coupled by the laser. For additional details about the resulting equations please refer to [30].

Both the pump and probe are linearly polarized, have the same frequency ω_0 and propagate along the z axis. As schematically given in figure 2, the probe laser beam is at the centre of the coaxial hollow pump beam. The initial probe beam radial profile is a Gaussian

$$I_{\mathrm{probe}}(r) = 2\bar{I}_{\mathrm{probe}}\exp\left(-2r^2/r_0^2\right), \tag{5}$$

where r_0 is the $1/e^2$ radius of the probe beam and $\bar{I}_{\mathrm{probe}}$ is the probe beam's intensity (total probe power divided by $r_0^2\pi$). The pump beam's intensity profile along the radial distance r is modelled as

$$I_{\mathrm{pump}}(r) = \bar{I}_{\mathrm{pump}}a(\mathrm{erf}(p(r-r_1)) - \mathrm{erf}(p(r-r_2))), \tag{6}$$

where $\bar{I}_{\mathrm{pump}}$ is the pump beam's intensity, a is the normalization constant, p affects the steepness of the profile near the beam's edge determined by the parameters r_1 and r_2.

It is assumed that every collision with the cell wall resets the state of an atom. Therefore, the atoms entering the pump beam from the direction of the wall have equally populated Zeeman sublevels of both hyperfine levels of the ground state. The density of the rubidium vapour at room temperature is low enough, so that Rb–Rb collisions are negligible. Therefore, an atom moves through the laser beams with constant velocity $\mathbf{v} = \mathbf{v}_\parallel + \mathbf{v}_\perp$, where $\mathbf{v}_\parallel$ and $\mathbf{v}_\perp$ are velocity components parallel and perpendicular to the direction of laser propagation, respectively. When calculating the density matrix at a given value of z, we neglect longitudinal changes of the beam profiles compared to the transverse ones so that only the transverse direction of the trajectory matters. From the reference frame of the moving atom, the electric field varies and the rate of variation depends only on $\mathbf{v}_\perp$. Assume that the transverse projection of the atomic trajectory at some z is given by $\mathbf{r}_\perp(t) = \mathbf{r}_{0\perp} + \mathbf{v}_\perp t$, where $\mathbf{r}_{0\perp}$ is the transverse component of the atom position vector at $t = 0$. The temporal variation of the laser intensity seen by the atom is given by

$$I(t, z) \equiv I(\mathbf{r}_\perp(t), z) = I(\mathbf{r}_{0\perp} + \mathbf{v}_\perp t, z), \tag{7}$$

corresponding to the transverse laser intensity variation along the trajectory of the atom in the laboratory frame. Additionally, due to cylindrical symmetry of the beam profiles, the transverse dependence becomes a purely radial dependence.

The observed experimental resonances are the probabilistic average of contributions due to many individual, mutually non-interacting Rb atoms. The atoms traverse the laser beams at different paths with different velocities. The Maxwell–Boltzmann velocity distribution, diversity of atomic trajectories and custom cylindrical symmetric radial beam profiles are treated similarly as in [30]. Atomic trajectories having different distances from the centre of the probe beam are chosen so that the probe beam's cross-section is uniformly covered. For a suitable set of atomic velocities, the atomic density matrix $\hat{\rho}(B; \mathbf{v}; \mathbf{r})$ along a given trajectory is calculated assuming constant magnetic field B during the atomic transit through the laser beams. Numerical integration of the optical Bloch equations is carried out from the moment when the atom enters the pump beam's region until it exits the probe beam. To obtain the atomic ensemble density matrix $\hat{\rho}(B; r, z)$ across the beam's cross-section at some z and for a set of radial distances r, the calculated density matrices are averaged over the Maxwell–Boltzmann velocity distribution and integrated over trajectories containing points at given radial distance r.

The velocity-averaged density matrix will possess cylindrical symmetry arising from the cylindrical symmetry of the laser beam profiles and the atomic velocity distribution. Thus, the angular integral appearing in the averaging over velocity $\mathbf{v}(\theta) = (\theta, v_\perp, v_\parallel)$ can be replaced by an angular integral over space

$$\hat{\rho}(B; r, z) = \int_0^{2\pi} \frac{\mathrm{d}\theta}{2\pi} \int_0^\infty \mathrm{d}v_\perp W_\perp(v_\perp) \int_{-\infty}^\infty \mathrm{d}v_\parallel W_\parallel(v_\parallel) \times \hat{\rho}(B; 0, v_\perp, v_\parallel; r\cos\theta, r\sin\theta, z), \quad (8)$$

with the Maxwell–Boltzmann velocity distribution given by

$$W_\perp(v_\perp) = \frac{2v_\perp}{u^2} \mathrm{e}^{-(v_\perp/u)^2}, \qquad W_\parallel(v_\parallel) = \frac{1}{u\sqrt{\pi}} \mathrm{e}^{-(v_\parallel/u)^2}, \quad (9)$$

where $u = (2k_BT/m_{\mathrm{Rb}})^{1/2}$ is the most probable velocity.

In order to make a comparison with the experiment, we calculate the transmission and the angle of the polarization rotation of the linearly polarized probe laser's light as a function of the magnetic field. The effects of the probe beam's propagation and variation in its intensity along the Rb cell are treated using

$$\frac{\partial \mathbf{E}(B; r, z)}{\partial z} = \frac{\mathrm{i}\omega_0}{2\epsilon_0 c} \mathbf{P}(B; r, z), \quad (10)$$

where ϵ_0 is the vacuum dielectric constant and c the speed of light in vacuum. The accompanying initial condition is given by (5) and by the angle of the probe's incident linear polarization. The Rb vapour ensemble density matrix $\hat{\rho}(B; r, z)$ at some values of z is computed using the electric field $\mathbf{E}(B; r, z)$. The polarization of the Rb vapour is obtained from the ensemble density matrix

$$\mathbf{P}(B; r, z) = n(T)\mathrm{Tr}(\hat{\rho}(B; r, z)\hat{\mathbf{d}}), \quad (11)$$

where the ^{87}Rb concentration $n(T)$ at absolute temperature T is taken from [31]. Due to the trace operation including the dipole operator $\hat{\mathbf{d}}$, the polarization $\mathbf{P}$ depends only on the optical coherences between the ground and excited Zeeman sublevels. Using the computed Rb polarization, we are able to calculate the change of the probe's electric field due to propagation through the Rb vapour from (10). Following that procedure, we calculate the transmitted electric field $\mathbf{E}(B; r, z = L)$, where L is the cell length, used in the calculation of the transmission and the angle of the polarization rotation of the probe laser beam. During the calculation of the probe beam's propagation, we also treated the pump beam's propagation effects in an analogous manner.

The angle of the polarization's rotation is calculated in a similar manner as measured from signals of the two detectors S_1 and S_2 behind the polarizing beam-splitter rotated at 45° with respect to the incident probe's polarization. The polarization's rotation angle is given by

$$\varphi = \frac{1}{2} \arcsin \frac{S_1 - S_2}{S_1 + S_2}. \quad (12)$$

Values of S_1 and S_2 were obtained from

$$S_{1,2} = \int_{S_p} |\mathbf{u}_{1,2} \cdot \mathbf{E}(B; r, z = L)|^2 \mathrm{d}^2\mathbf{r}, \quad (13)$$

where $\mathbf{u}_{1,2} = (\sqrt{2}/2)(\mathbf{e}_x \pm \mathbf{e}_y)$ are unity vectors corresponding to the polarizing beam splitter's, s and p, polarization axes and S_p is the probe beam's cross-section.

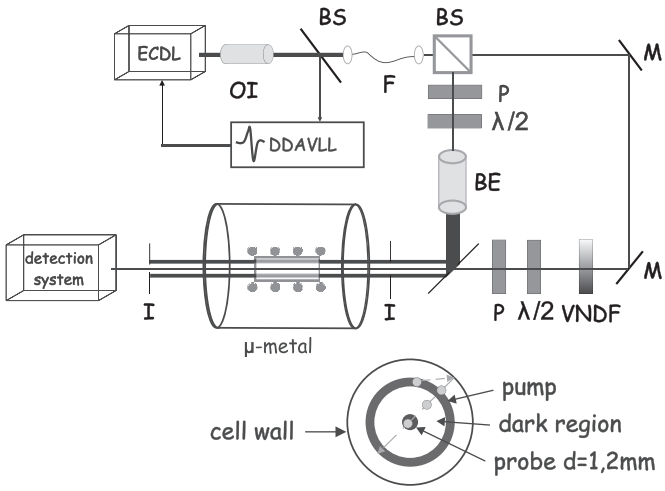

Figure 3. Experimental setup: ECDL-external cavity diode laser, OI-optical isolator, DDAVLL-Doppler free dichroic atomic laser lock, BS-beam splitter, F-optical fibre, M-mirrors, I-iris, P-polarizer, VNDF-variable neutral density filter, BE-beam expander, $\lambda/2$-retardation plate. Inset: transverse cross-section of the Rb cell with typical atomic trajectory.

3. Experimental setup

Figure 3 shows the experimental setup. An external cavity diode laser with a linewidth of about 1 MHz was used in the experiment. The laser frequency was locked to the D_2 transition $F_g = 2 \rightarrow F_e = 3$, in ^{87}Rb, using the Doppler-free dichroic atomic vapour laser lock (DDAVLL) technique [33]. The Gaussian laser beam is split into two beams, the pump beam and the probe beam. The diameter of the pump beam is enlarged and sent through a 12 mm diameter iris. The linear polarizations of the pump and probe beams, and the angle between their polarizations, are adjusted by a linear polarizer and $\lambda/2$ retardation plate. The important element for generating a laser beam like a hollow cylinder, as shown in figure 3(b), is a mirror with a hole [34]. The diameter of the hole thus determines the inner diameter of the hollow pump beam. We used two mirrors with central holes of 5 and 7 mm in diameter, respectively. The probe beam, 1.2 mm in diameter, comes from behind the mirror and passes through the hole's centre. The vacuum Rb gas cell is 85 mm long and its diameter is 25 mm. The cell is at room temperature. A scanning magnetic field along the laser beam's propagation is generated by the solenoid around the gas cell. Magnetic shielding from stray laboratory fields is achieved by three layers of μ-metal cylinders around the Rb cell. Behind the cell, the probe beam first passes through a pair of irises (in order to minimize the contribution of the pump beam) and then passes through the polarizing beam splitter with the fast axis oriented at 45° with respect to the direction of the initial polarization of the probe beam. Two beams emerging from the polarizing beam splitter were detected with two photodiodes. The sum $S_1 + S_2$ and the difference $S_1 - S_2$ of these two signals were recorded by a digital oscilloscope, while B was scanned around its zero value. The sum signal gives Hanle EIA, while the difference

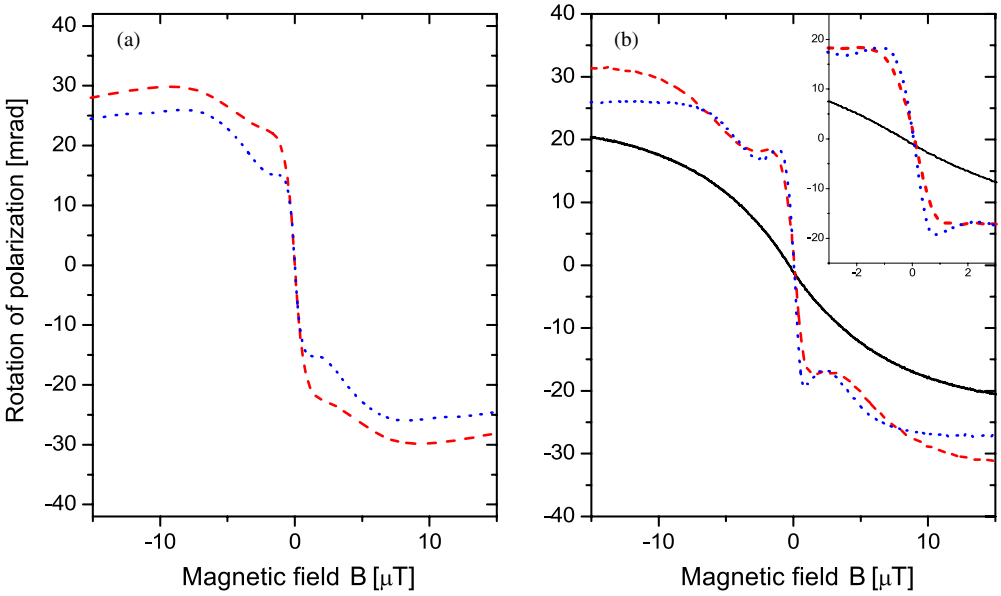

Figure 4. Calculated (a) and measured (b) probe NMOR for the $F_g = 2 \rightarrow F_e = 3$ transition in ^{87}Rb as a function of the axial magnetic field B. Dashed and dotted lines are for two inner pump beam diameters of 5 and 7 mm (corresponding to the 'dark region' size of 2 and 3 mm), respectively. Both pump and probe beams have the same linear polarization. The probe laser power is 10 μW, while the pump laser power is 1.2 mW. Solid line in (b) is NMOR for single wide laser beam having power of 10 μW and diameter of 7 mm. Inset in (b) shows the recorded resonances near $B = 0$.

signal gives NMOR. In this configuration, the rotation angle of the probe's polarization is given by

$$\phi = \frac{1}{2} \arcsin \frac{S_1 - S_2}{S_1 + S_2}. \tag{14}$$

4. Discussion

In this section, we present results concerning the probe laser's transmission and polarization rotation when the probe laser interacts with Rb atoms prepared into coherent superposition of Zeeman sublevels of the $F_g = 2$ ground hyperfine level by the spatially separated pump beam. We intend to demonstrate that the Ramsey effects play a role here as they do for dark resonances [22] by measuring and calculating the line-shapes of EIA and NMOR resonances for different sizes of the dark region, and for different atomic states generated by the pump beam. Both probe and pump beams are linearly polarized and resonant to the $F_g = 2 \rightarrow F_e = 3$ transition in ^{87}Rb. The pump beam fills almost the entire 25 mm diameter Rb cell except for the hole at its centre, which is either 5 or 7 mm in diameter. The probe beam of 1.2 mm in diameter is collinear with the pump beam and passes along the axis of the hollow pump beam. This configuration allows, like in the Rb cells with anti-relaxation coating or buffer gas, repeated interaction of atoms and laser fields. It provides higher influx of atomic states prepared by the pump beam that reach the probe beam passing through the central hole, in comparison with co-propagating parallel but spatially separated Gaussian laser beams in [21]. In addition, the use of two separate laser beams gives the ability to independently control the properties of the beams, like polarization and power. Our experimental geometry is similar to the geometry used in [32], where the sub-Doppler feature was observed in the transmission of the hollow probe, through the very thin (10 μm) cell, while the pump beam is placed in the centre of the probe.

We first present theoretical and experimental line-shapes of the probe's NMOR, calculated and measured from the signals at the two detectors of the balanced polarimeter as a function of the external magnetic field B. The direction of the magnetic field is along the laser beam's propagation. In the experiment, the magnetic field varies slowly (50 Hz) so that the period of a magnetic sweep is much longer than typical atom transit time across the cell. This validates the assumption made in the theoretical model that B is constant while the atom passes through three regions of the Rb cell: the pump laser beam, the dark region and the probe laser beam. In all figures, spatially displaced pump and probe beams have the same frequency. Figures 4(a) and (b) present the calculated and measured angle of rotation of the linear probe polarization as a function of the axial magnetic field. The linear polarizations of the pump and probe beams are parallel. When the pump laser is turned on, the probe's NMOR resonance has a central dispersive shape and a pair of much weaker sidebands around the centre. Results are given for the two inner diameters of the pump beam, 5 and 7 mm. The resonance width decreases with the distance between the pump and the probe laser beam, which is a characteristic of the Ramsey effect. For dark regions of sizes 2 and 3 mm, the NMOR width is 2.4 and 1.6 μT, respectively. The results given in figures 4(a) and (b) show good agreement between theoretical predictions and experimental measurements. The solid curve in figure 4(b) corresponds to NMOR resonance of a single wide laser beam of 7 mm in diameter and 10 μW of power. It is notably wider and has smaller amplitude than the probe resonances obtained in pump–probe configuration, although the probe beam's diameter is much smaller, 1.2 mm. The amplitudes of NMOR and EIA are larger than for an open

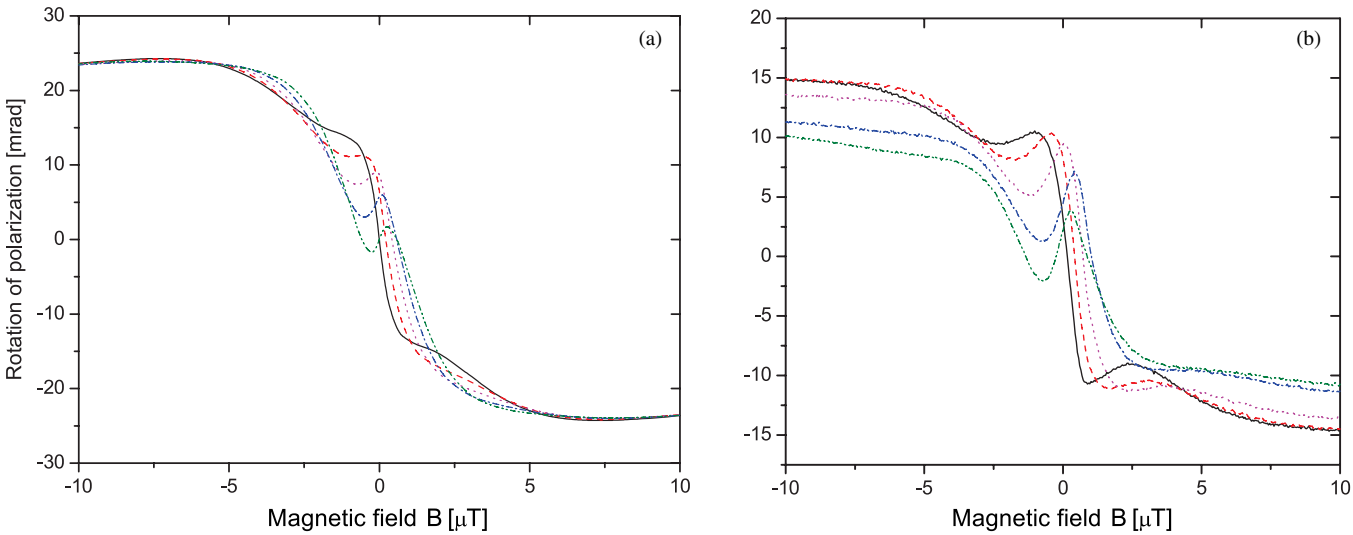

Figure 5. Theoretical (a) and experimental (b) results for the angle of rotation of the probe polarization for different angles between linear polarization of the pump and probe beams (0° black, 22.5° red, 45° green, 67.5° blue and 90° magenta). The pump and probe beams couple the $F_g = 2 \rightarrow F_e = 3$ transition in ^{87}Rb. The probe and pump laser powers are 20 μW and 1.2 mW, respectively. The pump beam's inner diameter is 7 mm.

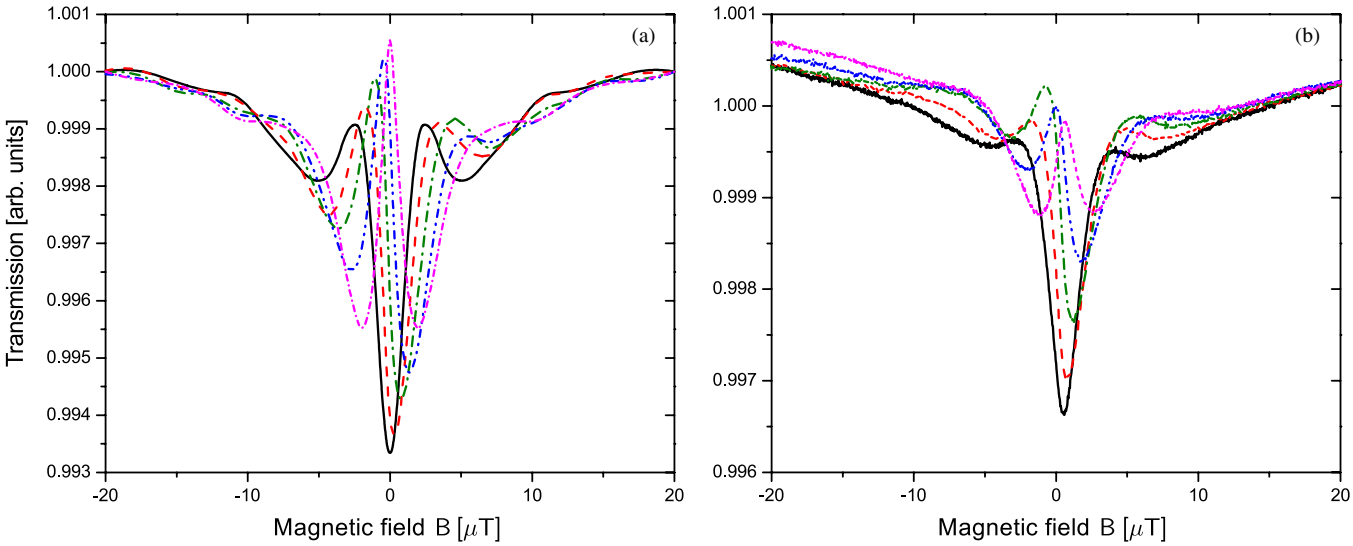

Figure 6. Theoretical (a) and experimental (b) results of the probe's absorption spectra for the $F_g = 2 \rightarrow F_e = 3$ transition in ^{87}Rb, for linearly polarized pump and probe beams and different probe beam polarization angles with respect to the pump beam's polarization (0° black, 22.5° red, 45° green, 67.5° blue and 90° magenta). The probe and pump powers are 20 μW and 1.2 mW, respectively. The pump beam's inner diameter is 7 mm.

EIT transition [23] because the closed transition limits losses of population to the hyperfine level of the uncoupled ground state.

The initial phases of atomic ground state coherences created in the pump beam can be controlled by varying the relative angle between pump and probe beam polarizations. Rotating the polarization of the pump beam by the angle φ, the phase between the circular components of the pump beam is changed by 2φ. This leads to the change of the phase of the atomic ground state coherences entering the probe beam by 2φ, for a constant magnetic field. In figure 5, we present the results for the probe beam's polarization rotation for several angles between the electric vectors of linearly polarized pump and probe beams. When we set the angle between the two electric field vectors to $\varphi = \pi/2$, we obtain the opposite sign for the probe beam's polarization rotation ($2\varphi = \pi$). For the angle φ between 0 and $\pi/2$, the dispersion-like curves for the probe NMOR beam are centred at an external magnetic field different from zero. The magnetic field corresponding to the centre of the NMOR resonance increases with the angle between the polarizations of two beams because different phases of the coherence require a different magnetic field for the constructive interference to occur. The comparison between results in figures 5(a) and (b) shows that calculated and measured line-shapes have very similar behaviour.

Figure 6 presents the Ramsey interference effects on the shape of EIA resonances. It shows the probe beam's transmission for several angles between the electric vectors

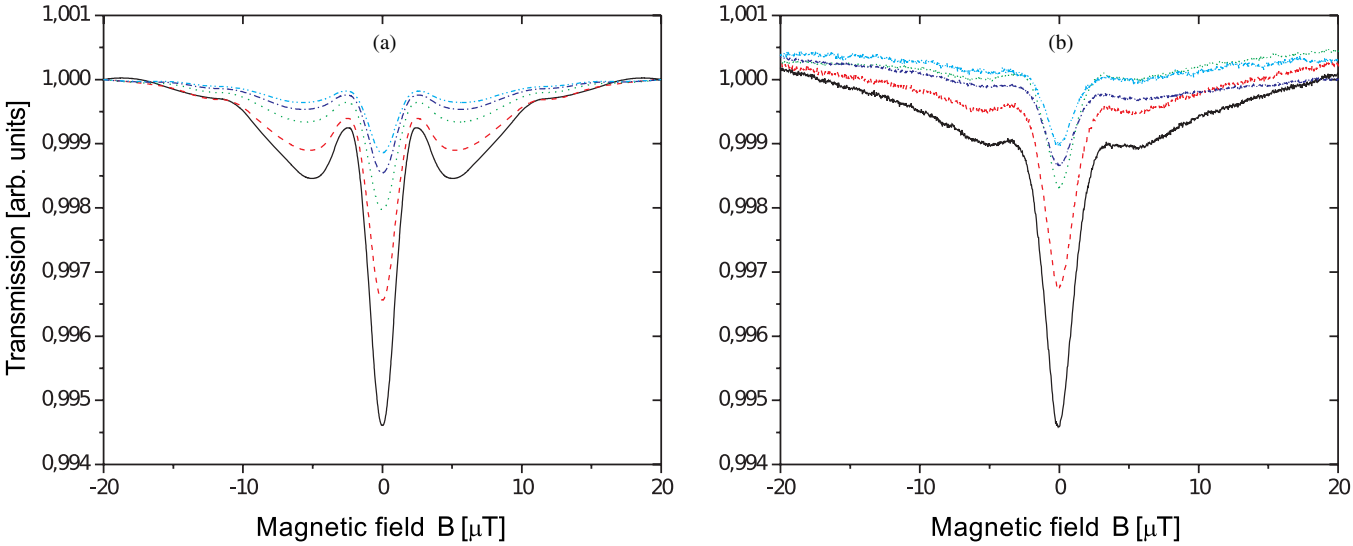

Figure 7. Theoretical (a) and experimental (b) results of the probe's absorption spectra for the $F_g = 2 \rightarrow F_e = 3$ transition in ^{87}Rb, for linearly polarized pump and probe beams and different powers of the probe beam (10 μW solid, 20 μW dashed, 40 μW dotted, 60 μW dash-dot, 80 μW dash-dot-dot lines). The pump laser power is 1.2 mW. The inner pump beam's diameter is 7 mm.

of linearly polarized pump and probe beams. Interference between the coherently prepared atoms and the probe field will give a probe transmission dip (for $2\varphi = 0$) or transmission gain (for $2\varphi = \pi$) around the same magnetic field values. These two cases are presented by solid and dash-dot-dot lines, respectively. For other values of φ, the transmission has a dispersion-like shape. As the angle between two polarizations increases, the main transmission dip shifts towards higher values of B, since a larger magnetic field is necessary for the occurrence of constructive interference. The comparison between the results in figures 6(a) and (b) shows that calculated line-shapes are very similar to the measured line-shapes. Similar dispersion-like line-shapes for an arbitrary angle between the linear polarizations of two laser fields have been theoretically predicted for EIA in a bichromatic laser field [35]. The behaviour observed from figures 5 and 6 supports the fact that the atomic ground state coherences essentially determine the development of EIA and NMOR in the considered atomic system.

The effects of the probe laser's power on the probe's transmission are given in figure 7. Both theory and experiment show that the increase of the probe beam's power lowers the amplitudes of the narrow central transmission dip. Higher probe beam power increases the probe beam's contribution to EIA resonance and at the same time lowers the effects of the pump beam induced atomic coherence. As long as the effect of atomic coherence entering the probe beam dominates over the probe's contribution, the resonance width of the central dip remains the same.

5. Conclusion

Experimental and theoretical evidences imply that probe EIA and NMOR in a vacuum Rb gas cell at room temperature are strongly affected by interference effects between the probe beam and atomic states prepared by the spatially separated pump beam in the presence of a small magnetic field. By increasing the size of dark region between the pump and probe, the resonances become narrower. By changing the initial phase of the atomic coherence in the pump beam, fully constructive interference with the probe beam can change into fully destructive interference yielding the change of the sign of the resonances. Moreover, the Ramsey effects seem to be even more pronounced on the EIA linewidth and amplitude than for EIT (developed on atomic transition $F_g \rightarrow F_e = F_g - 1$), as found by comparing the results for both phenomena using the same geometry of the laser beams [22, 23]. Among many differences between EIT and EIA, these results show that the response of ground state Zeeman coherences in an atomic system showing EIA to Ramsey-type excitation is very similar to the previously observed response of Zeeman coherences in atomic systems showing EIT [22, 23].

Acknowledgments

This work was supported by the Ministry of Education and Science of Serbia, under grant nos III45016 and OI171038 and also by SCOPES JRP IZ73Z0_127942.

References

[1] Akulshin A M, Barreiro S and Lezama A 1998 *Phys. Rev.* A **57** 2996
[2] Kazantsev A, Smirnov V, Tumaikin A and Yagofarov I 1984 *Opt. Spectrosc. (USSR)* **57** 116
Kazantsev A, Smirnov V, Tumaikin A and Yagofarov I 1984 *Opt. Spektrosk.* **57** 189
[3] Harris S E 1997 *Phys. Today* **50** 36
[4] Arimondo E and Orriols G 1976 *Lett. Nuovo Cimento Soc. Ital. Fis.* **17** 333
[5] Lezama A, Barreiro S and Akulshin A M 1999 *Phys. Rev.* A **59** 4732
[6] Dancheva Y, Alzetta G, Cartaleva S, Taslakov M and Andreeva C 2000 *Opt. Commun.* **178** 103

[7] Kim S K, Moon H S, Kim K and Kim J B 2003 *Phys. Rev.* A **68** 063813
[8] Brazhnikov D V, Tumaikin A M, Yudin V I and Taichenachev A V 2005 *J. Opt. Soc. Am.* B **22** 57
[9] Dimitrijević J, Arsenović D and Jelenković B M 2007 *Phys. Rev.* A **76** 013836
[10] Dimitrijević J, Krmpot A, Mijailović M, Arsenović D, Panić B, Grujić Z and Jelenković B M 2008 *Phys. Rev.* A **77** 013814
[11] Dimitrijević J, Grujić Z, Mijailović M, Arsenović D, Panić B and Jelenković B M 2008 *Opt. Express* **16** 1343
[12] Failache H, Valente P, Ban G, Lorent V and Lezama A 2003 *Phys. Rev.* A **67** 043810
[13] Taichenachev A V, Tumaikin A M and Yudin V I 1999 *Phys. Rev.* A **61** 011802
[14] Dimitrijević J, Arsenović D and Jelenković B M 2011 *New J. Phys.* **13** 033010
[15] Valente P, Failache H and Lezama A 2003 *Phys. Rev.* A **67** 013806
[16] Akulshin A M, Barreiro S, Sidorov A I, Hammaford P and Opat G I 2003 *Phys. Rev.* A **67** 011801
[17] Akulshin A M, Sidorov A I and Hannaford P 2006 *Phys. Rev.* A **73** 033806
[18] Goren C, Wilson-Gordon A D, Rosenbluh M and Friedmann H 2003 *Phys. Rev.* A **67** 033807
[19] Ramsey N 1956 *Molecular Beams* (London: Oxford University Press)
[20] Xiao Y, Novikova I, Phillips D F and Walsworth R L 2006 *Phys. Rev. Lett.* **96** 043601
[21] Zibrov A S and Matsko A B 2001 *Phys. Rev.* A **65** 013814
[22] Grujić Z D, Mijailović M, Arsenović D, Kovacević A, Nikolić M and Jelenković B M 2008 *Phys. Rev.* A **78** 063816
[23] Mijailović M M, Grujić Z D, Radonjić M, Arsenović D and Jelenković B M 2009 *Phys. Rev.* A **80** 053819
[24] Kim H-J and Moon H S 2011 *Opt. Express* **19** 168
[25] Kim H-J and Moon H S 2012 *Opt. Express* **20** 9485
[26] Barkov L M, Melik-Pashayev D and Zolotorev M 1989 *Opt. Commun.* **70** 467–72
[27] Kanorsky S I, Weis A, Wurster J and Hänsch T W 1993 *Phys. Rev.* A **47** 1220
[28] Budker D, Kimball D F, Rochester S M and Yashchuk V V 2000 *Phys. Rev. Lett.* **85** 2088
[29] Budker D, Gawlik W, Kimball D F, Rochester S M, Yashchuk V V and Weis A 2002 *Rev. Mod. Phys.* **74** 1153
[30] Radonjić M, Arsenović D, Grujić Z and Jelenković B M 2009 *Phys. Rev.* A **79** 023805
[31] Nesmeyanov A N 1963 *Vapour Pressure of the Chemical Elements* (Amsterdam: Elsevier)
[32] Briaudeau S, Saltiel S, Leite J R R, Oria M, Weis A, Bloch D and Ducloy M 2000 *J. Phys.* IV *France* **10** Pr8–145
[33] Corwin K L, Lu Z T, Hand C F, Epstein R J and Wieman C E 1998 *Appl. Opt.* **37** 3295
[34] Chang Chun Bo Xin Photoelectric Co. Ltd. (Chang Chun, Ji Lin, China), www.bxoptic.com/
[35] Zhukov A A, Zibrov S A, Romanov G V, Dudin Y O, Vassiliev V V, Velichansky V L and Yakovlev V P 2009 *Phys. Rev.* A **80** 033830